

Brine rejection and crystallite formation upon freezing NaCl aqueous solutions

Ifigeneia Tsironi^{1,a)}, Daniel Schlesinger², Alexander Späh¹, Lars Eriksson³, Mo Segad³ and Fivos Perakis^{1,b)}

¹*Department of Physics, AlbaNova University Center, Stockholm University, S-10691 Stockholm, Sweden*

²*Department of Environmental Science and Analytical Chemistry & Bolin Centre for Climate Research, Stockholm University, 114 18 Stockholm, Sweden*

³*Department of Materials and Environmental Chemistry, Stockholm University, Sweden*

a)Present address: Department of Chemistry, University of Miami, Coral Gables, Florida 33146, United States

b)Author to whom correspondence should be addressed: f.perakis@fysik.su.se

ABSTRACT

Studying the freezing of saltwater is of fundamental importance for improving cryo-desalination methods, as well as for modeling arctic ice and iceberg dynamics. Here, we probe with x-ray diffraction the freezing process in NaCl solutions for different salt-water concentrations, ranging from seawater conditions to brine. A simple linear superposition model can well reproduce brine rejection due to ice Ih formation and allows us to quantify the ratio between brine and ice. In addition, we perform molecular dynamics simulations to model the formation of NaCl crystallites and we observe signatures of ion-water cross-correlations due to ion inclusion within the ice Ih lattice evident in the diffraction pattern. This study demonstrates a sensitive method of detecting salt trapped inside the ice in the form of crystallites and can provide valuable insight to improve desalination efficiency from a molecular perspective.

I. INTRODUCTION

Water is the most abundant liquid on earth and is known for its importance in many chemical, biological and geological processes, but also for its many unusual thermodynamic and structural properties¹⁻⁴. Despite being one of the most studied liquids, understanding the role of water in biochemical systems continues to be a great challenge^{5,6}. Most of the water found in nature has a considerable amount of salt, since approximately 96.5% of the earth's water is within the ocean⁷. Among the salts found in seawater, sodium chloride (NaCl) is the main ionic component. Understanding the NaCl aqueous solutions can have very broad implications, ranging from biochemical applications to atmospheric science modeling⁸⁻¹¹.

Seawater forms ice upon cooling, which covers up to 12% of the surface of the oceans¹². Understanding the freezing process of seawater is very important for modeling the arctic ice dynamics that influence oceanic circulation and climate change. The freezing temperature of the salt solution is lowered upon increasing NaCl concentration and thus the region where water can be supercooled is extended¹³. By using salt solutions one can study the properties of water in the deeply supercooled regime¹⁴⁻¹⁸, as ions can prevent crystallization, which can lead to the observation of a liquid-liquid transition in supercooled aqueous solutions¹⁹. When the freezing process of such solutions takes place, the salt ions are rejected from the solid phase, due to the preferential formation of pure ice. As a result the remaining liquid phase turns into what often is referred to as *brine*, which is liquid water saturated with salt^{20,13}. This phenomenon, called *brine rejection*, ultimately leads to separation of salt from ice formed during the freezing process. Brine rejection triggers massive oceanic flow which influences the circulation of the high-latitude ocean and thus affects the global climate^{21,22}. Probing on a molecular level the water-salt separation induced by crystallization can facilitate the development of effective methods for acquiring fresh water from seawater via desalination. The salting-out occurring due to freezing is one of the basic mechanisms in *cryo-desalination*, also known as *freezing-melting* and

freeze-thaw desalination²³⁻²⁵. The main challenge is the ice-brine separation, i.e. the separation of salt from crystalline ice due to the formation of polycrystalline micro-domains forming upon crystallization.

Brine rejection is apparent in sea ice and influences its mechanical, electromagnetic and transport properties²⁶. It has been shown that brine rejection occurs through brine channels, that are liquid conducts extending through the ice.²⁶ The diameter of the channels forming and thus the quantity of the salt rejected, depends on the freezing temperature²⁷. It is often assumed that the salt does not enter the crystal structure but that the salt molecules are being expelled and collected within the brine solution that forms the channels²⁸. Experiments indicate that frozen NaCl aqueous solutions can form many NaCl-water crystal phases^{29,30}. In addition, theoretical investigations indicate that on a molecular level, brine rejection progresses through a disordered layer with fluctuating ion density, followed by a neat ice layer³¹. Recent simulations further indicate that salt is included in the ice lattice as dopant, with Cl⁻ ions having higher probability of inclusion than Na⁺ ions^{32,33}. Furthermore, in the case of homogeneous nucleation of salty water, the nucleation rate decreases with addition of salt¹⁸.

The physics of salt water freezing is portrayed by the temperature-concentration phase diagram, depicted in Fig. 1. The salt solution is in liquid form at temperatures above the melting point and low concentration of NaCl, whereas increase of salt concentration beyond saturation initiates the formation of NaCl crystals. Upon decreasing temperature, ice Ih (hexagonal) formation occurs leading to brine rejection, which coexists with the ice crystals. The three phases meet at the so called *eutectic point* of NaCl³⁴ located at a concentration of 3.99 M (23.3% m/m) and a temperature of -21.1°C. Upon further cooling, the salt solution crystallizes and it is commonly assumed that it consists of a mixture of salt and ice crystals.

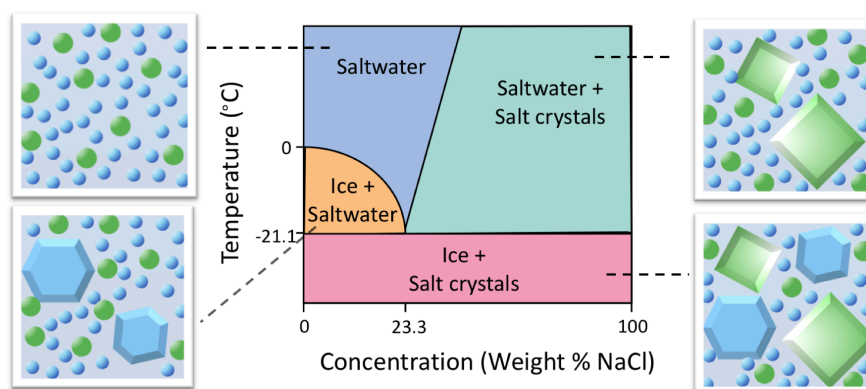


FIG. 1 A schematic phase diagram of NaCl aqueous solution. Above the melting point and in low concentration of NaCl the solution is in liquid phase. At higher concentrations, saturation is reached and salt crystals coexist with saltwater. Upon decreasing the temperature below the melting point, ice Ih is formed pushing out the salt, in a process called brine rejection. When decreasing the temperature below -21.1°C, ice Ih and salt crystals coexist.

In this work, we investigate both experimentally and theoretically the crystallization of NaCl aqueous solutions and the brine rejection process using X-Ray Diffraction (XRD) for different temperatures and NaCl concentrations, across the phase diagram. A model is devised based on a linear superposition of saltwater, ice and salt crystals. Even though the model quantitatively reproduces the brine and ice coexistence, it does not capture the regime where ice and salt crystallites coexist and, in particular it does not predict all peaks observed in the diffraction pattern. The analysis is complemented by molecular dynamics (MD) simulations and the radial distribution functions are calculated for both water-water, water-ion and ion-ion correlations. The MD simulation indicate that the additional peaks in the XRD pattern not predicted by the simple linear model arise from ion-water interference during the formation of salt crystallites and from ions enclosed in the ice lattice. As a result, the combination of the linear model with the MD simulations provide a molecular insight to the brine rejection mechanism investigated by XRD and allows us to estimate the cryo-desalination efficiency.

II. METHODS

A. Experimental methods

The NaCl aqueous solutions were prepared at different concentrations using the mass percent solutions (m/m). The NaCl solute employed was laboratory-grade reagent purchased by Sigma Aldrich and used without further purification in combination with MilliQ water. Each sample of different mass concentration was inserted in a quartz capillary (diameter 1mm, wall thickness 10 μm) and sealed with capillary wax. An X-ray diffractometer Bruker D8 VENTURE was used for the diffraction data using a Molybdenum source ($\lambda = 0.7107 \text{ \AA}$). An identical protocol was applied for all NaCl solutions measured at several temperatures and concentrations. The temperature was regulated by a liquid nitrogen cryo-steam at the sample position.

B. Molecular dynamics methods

We performed molecular dynamics (MD) simulations using the GROMACS package³⁵ (ver. 5.1.4), to investigate the exclusion of ions from a growing ice crystal. We used the OPLS force field³⁶ for Na^+ and Cl^- ions together with the TIP4P model of water³⁷. All simulations were run with $N_{\text{H}_2\text{O}} = 13824$ TIP4P molecules and $N_{\text{Cl}^-} = N_{\text{Na}^+} = 100$ Na^+ and Cl^- ions, respectively, corresponding to an aqueous NaCl solution at a concentration of about 2.3 % (m/m) at temperatures of $T = 220 \text{ K}$. The melting temperature of the TIP4P model of water has previously been determined³⁸ to be $T_m = 232 \pm 5 \text{ K}$ and the simulation temperatures thus correspond to temperature differences from the melting point of pure TIP4P water of about $\Delta T = T - T_m = -12 \text{ K}$ at ambient pressure. Ice growth was initiated with an ice seed of $N_{\text{seed}}=3456$ molecules corresponding to crystal with dimensions of about $5.40\text{nm} \times 4.65 \text{ nm} \times 4.39 \text{ nm}$. The simulations were run in the NPT ensemble using the Bussi thermostat³⁹ and the Berendsen barostat⁴⁰ with semi-isotropic pressure coupling ($p_x = p_y \neq p_z$) to fix the rectangular geometry of the simulation box about $(5.40 \times 4.65 \times 17.59) \text{ nm}$. Coulomb interactions were treated using the particle-mesh Ewald method and real space Coulomb, whereas van der Waals interaction were taken smoothly to zero between 0.87 and 0.9 nm. In addition, we used dispersion corrections and simulations were run for $t_{\text{sim}} = 1 \mu\text{s}$ at a time step of $\Delta t = 2 \text{ fs}$ (Fig.2).

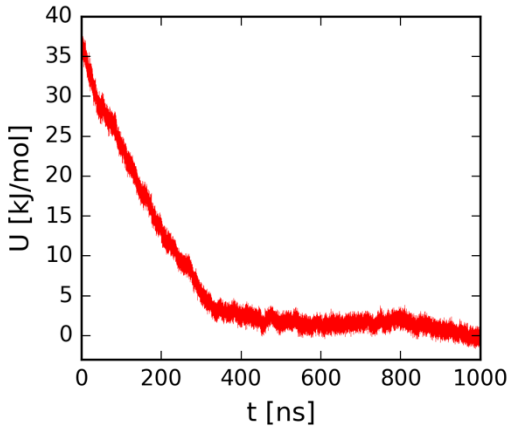


FIG. 2 Potential energy of the NaCl solution as a function of time at temperature $T = 220 \text{ K}$, which is below the melting temperature $T_m = 232 \pm 5 \text{ K}$ of the TIP4P water model.

III. RESULTS

A. Experimental results

X-ray diffraction scattering patterns were obtained for a series of salt solutions, as well as for pure water and pure NaCl crystals. The XRD patterns recorded at temperatures $T = 293$ K, $T = 260$ K and $T = 230$ K and concentration 0.86 M (5% m/m), shown in Fig.3. At $T = 293$ K, the scattering pattern is uniform and broad, indicative of the sample being in liquid form, i.e. salt water. At $T = 230$ K the appearance of sharp Bragg peaks indicates a crystalline structure arising from ice Ih and salt crystals. At the intermediate temperature $T = 260$ K, the scattering pattern exhibits coexistence of the liquid and crystalline forms manifested during the brine exclusion process. These three distinct structures observed correspond to different areas of the phase diagram presented in Fig.1.

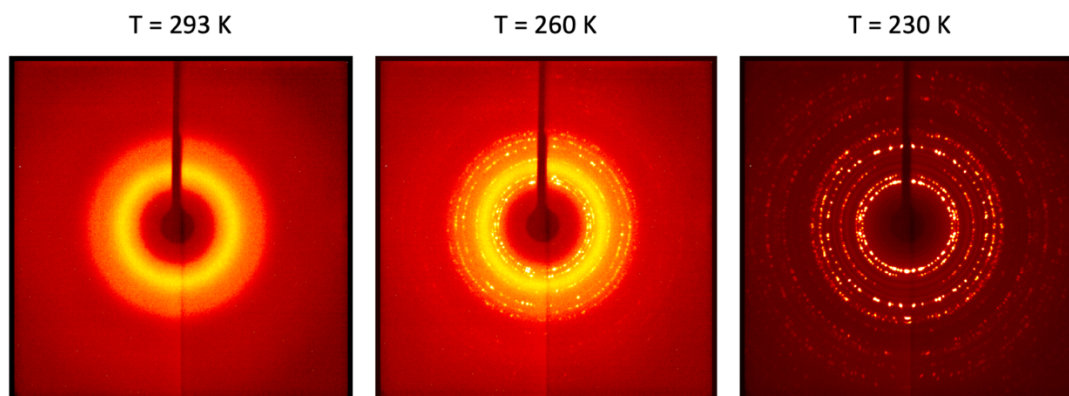


FIG. 3 X-ray scattering patterns of NaCl solutions at 0.86 M (5% m/m) at different temperatures. a) The NaCl solution at $T = 293$ K, evident by the broad halo peak. b) At $T = 260$ K water crystallization is seen by the appearance of sharp Bragg peaks overlaying the broad halo due to brine exclusion. c) At $T = 230$ K the diffraction pattern consist only of Bragg peaks indicating the presence of salt crystals and ice Ih.

The angularly integrated scattering intensity $I(Q)$ obtained for different salt concentrations, 0.86 M, 1.71 M, 2.57 M, 4.28 M (5% m/m, 10% m/m, 15% m/m, 25% m/m respectively) is shown in Fig. 4. Upon increasing concentration in the liquid at 293 K shown in Fig.4A, the first diffraction peak shifts and becomes less structured, in agreement with previous investigations^{41,42}. This change in the scattering pattern is indicative of the influence of salt on the structure of the hydrogen bond network of water, seen also by X-ray Absorption Spectroscopy⁴³ and Small-Angle X-ray Scattering⁴⁴. The scattering intensity at $T = 260$ K shown in Fig.4B, corresponds to ice Ih coexisting with brine. In this condition, it is evident that the intensity of the peaks depends strongly on the concentration of salt and one can observe a decrease in the peak intensity with increasing salt concentration. This is due to the fact that by changing the amount of salt present in the solution, one effectively changes the relative ratio of ice and brine, while the total scattering intensity is conserved. For lower salt concentrations, the solution consists mainly of ice Ih and results in sharp Bragg peaks. Upon increasing salt concentration the relative amount of brine increases, seen by the broad peak located at $Q = 2.1 \text{ \AA}^{-1}$.

For temperatures below 230 K the sample crystallizes completely and consists largely of a mixture of ice Ih and salt crystals, as can be seen in Fig.4C for different salt concentrations. Interestingly, upon increasing concentration, we observe the appearance of two new peaks at the lower momentum transfer region $Q = 1.11 \text{ \AA}^{-1}$ and $Q = 1.278 \text{ \AA}^{-1}$. The scattering pattern exhibits sharp Bragg peaks at this length scale, which are distinct from those present in the crystalline structure of ice Ih and the NaCl crystals.

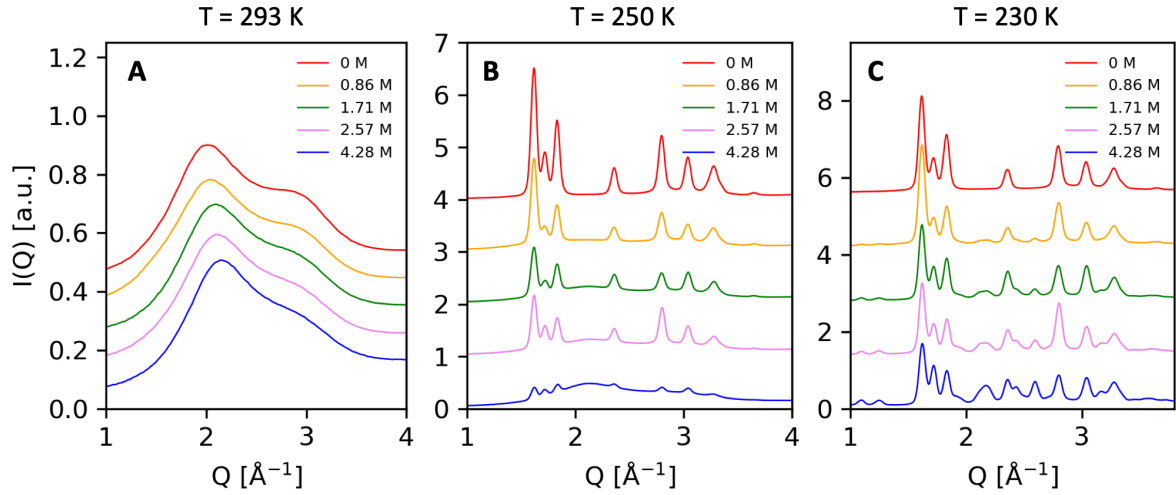


FIG. 4 Angularly integrated scattering intensity $I(Q)$ of NaCl solutions at various temperatures and concentrations. **A** Comparison of $I(Q)$ for different concentrations at temperature $T=293\text{K}$. **B** The $I(Q)$ for different NaCl concentration in ice Ih and brine conditions at temperature $T=250\text{K}$. **C**. The $I(Q)$ for different NaCl concentrations at temperature 230K , where the Bragg peaks arise predominantly from ice Ih and NaCl crystals.

B. Simulation results

Snapshots of the simulation at different times of the trajectory at $T = 220\text{K}$ are shown in Fig. 5. The Na^+ ions are denoted by dark blue spheres and Cl^- ions by turquoise spheres. Initially, the simulations were seeded with a slab of pure ice Ih with the basal plane exposed to the NaCl liquid solution ($t = 0$ ns). The crystallization rate is in the order of $20\text{ nm}/\mu\text{sec}$ at 220K and most of the ions “pushed” into the liquid form via brine exclusion. However, a small fraction of ions trapped inside the ice lattice, consistent with previous MD simulations³² where it was seen that more Cl^- is incorporated in the lattice than Na^+ . From the initial 200 ions, we observe that 19 are enclosed in the ice Ih lattice, 7 of which are Na^+ . Despite the limited statistics one can estimate that the ion concentration in ice due to inclusions is in the order of 0.5% m/m. This value is significantly reduced from the initial concentration 2.3% m/m, and near the standard salinity limits of fresh water, which is typically 0.1% m/m for drinking water and 0.5% m/m for agricultural use. The potential energy of the system (Fig.2) decreases rapidly upon ice growth and the decrease slows down at about 350 ns , when the salt concentration has reached sufficiently high values to prevent the liquid from further freezing. After this point, we observe the formation of small salt crystallites in the remaining liquid.

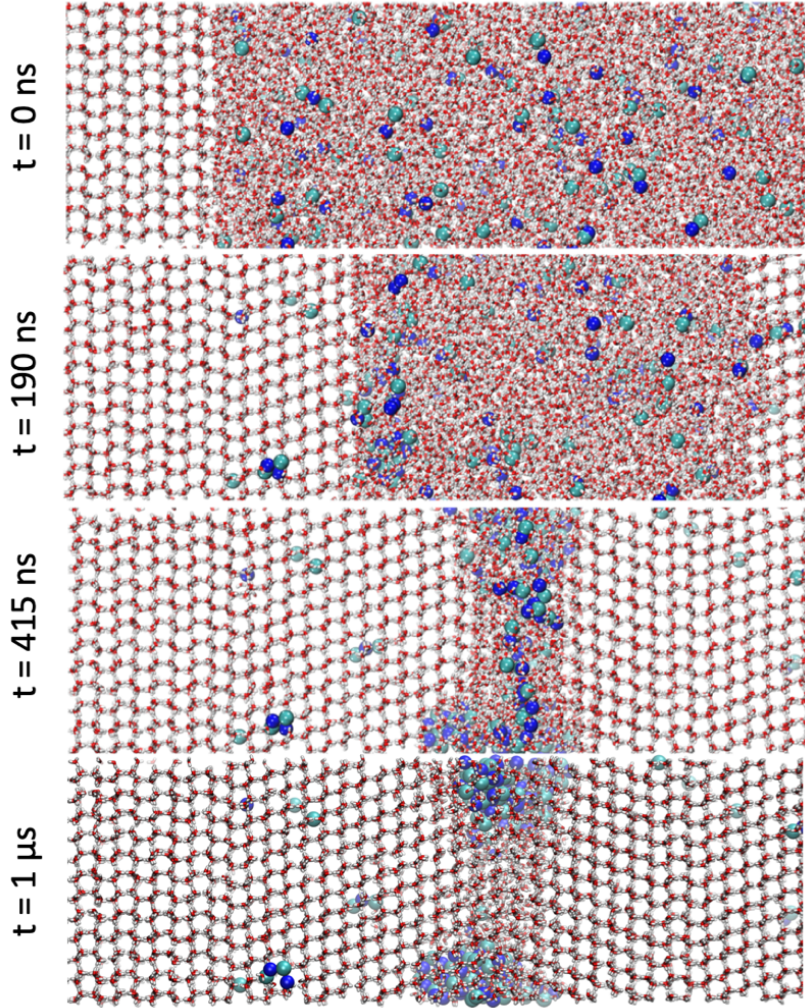


FIG. 5 Snapshots of a simulation box at $T = 220$ K showing ice crystal growth at times $t = 0$ ns, 190 ns, 415 ns and $1 \mu\text{s}$. Some ions get trapped within the ice structure while the majority of ions are expelled into the solution phase of increasing salt concentration. Na^+ ions are represented by dark blue, while Cl^- ions by turquoise spheres. The snapshots were rendered with VMD⁴⁵.

IV. DISCUSSION

In order to quantify the underlying contributions to the XRD diffraction pattern we construct a simple model comprising of a linear combination of the different components of each part of the phase diagram. Fig. 6A shows such an analysis for $T = 250$ K, where we observe coexistence of brine and ice Ih. The model utilizes two components shown in the upper row, where an offset has been introduced to facilitate the comparison. Here, the two components utilized are pure ice Ih measured at 250 K (blue solid line) and NaCl aqueous solution at $T = 293$ K with concentration 4.28 M (25% m/m) to mimic the saturated brine solution (orange solid line). The linear superposition of those two components is labeled as ‘model’ and is indicated with a dashed line. The relative amplitude of the two components can inform us about the ratio of crystalline ice Ih and brine concentration. When comparing this model with the data obtained at $T = 250$ K and concentrations 1.71 M (red solid line) and 4.28 M (green solid line) we observe good agreement with the experimental results. The ice Ih to brine ratio is estimated to be 0.4 for 1.71 M (10 % m/m) and 0.1 for 4.28 M (25 % m/m). One of the limitations of the model is that we use the NaCl aqueous solution at $T = 293$ K, whereas the data is taken at $T = 250$ K, which can introduce a shift in the first diffraction peak. An additional limitation of this approach is that this model does not include any interference (cross-terms) between the ice Ih and the brine, as the XRD pattern is the linear superposition of contributions arising from the two components. Despite those limitations, the model seems to capture all the diffraction peaks observed experimentally in the case of ice and brine coexistence (Fig. 6A).

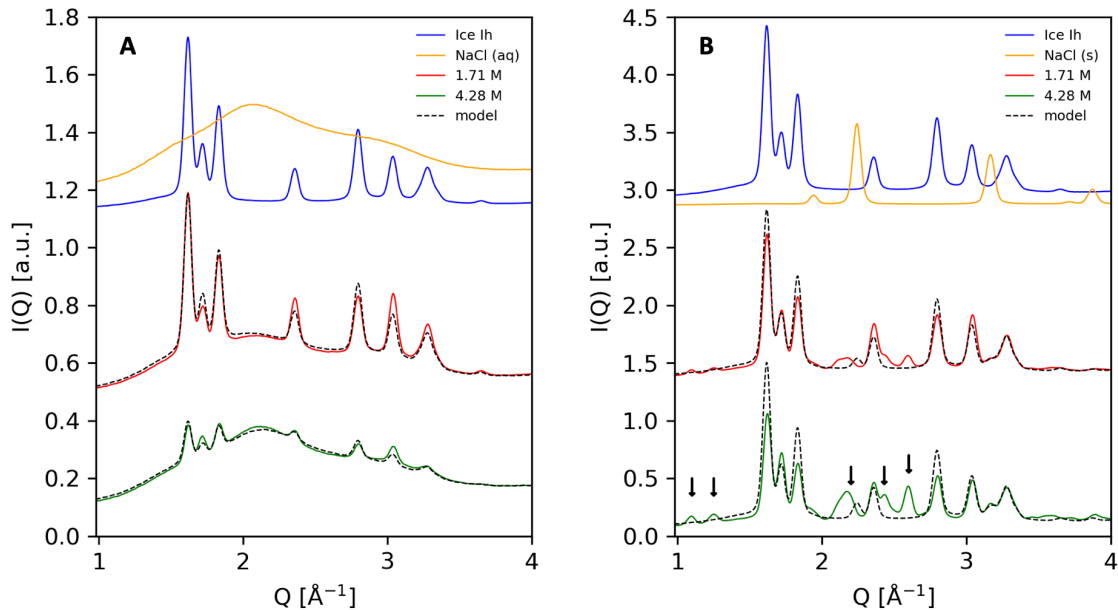


FIG. 6. A. A model based on linear superposition of the different components is used to analyze the $I(Q)$. The brine and ice coexistence at $T = 250$ K is modeled by combining ice Ih (blue solid line) with the NaCl aqueous solution at 4.28M (orange solid line). The linear combination ('model' dashed line) is compared to the data at $T=250$ K with concentration 1.71 M (10 % m/m) and 4.28 M (25 % m/m). **B.** The same analysis for $T = 230$ K, where the two components in this case consist of ice Ih (blue solid line) and NaCl crystals (orange solid line). The model (dashed line) is compared with the data recorded at concentrations 1.71 M (10 % m/m) and 4.28 M (25 % m/m).

A similar approach is used for the data at $T=230$ K, consisting of crystalline salt and ice Ih. The model consists of the NaCl crystal powder (Fig.6 B – orange solid line) and ice Ih recorded at $T = 230$ K (Fig. 6B – blue solid line). In this case the model (dashed line) does not reproduce all the peaks observed in the experiment for 1.71 M (red line) and 4.28 M (green line). There are several additional peaks not included in the simple model at $Q = 1.1 \text{ \AA}^{-1}$, 1.23 \AA^{-1} , 2.17 \AA^{-1} , 2.42 \AA^{-1} , 2.60 \AA^{-1} , depicted by the arrows. These new features indicate that in this region of the phase diagram, the system cannot be described through a simple superposition of salt crystals and ice Ih regions. Interestingly the peak position does not change with concentration and we only observe changes in the peak amplitude. The model does not contain any information about the water-salt interaction upon crystallization, that could lead to the observed peaks. Additionally, in the modeled XRD pattern the interference between water and salt is not included, which could also lead to additional contributions in the scattering intensity. Such interference could arise from the presence of salt inside the ice lattice or the between small salt crystallites and the surrounding water.

In order to further investigate the origin of the observed scattering components we utilize the MD simulations to calculate the radial distribution function $g(r)$ shown in in Fig. 7. Here a distinction is made between the self-correlations of the different atoms (Fig.7A and Fig.7B), such as the O-O, Cl-Cl and Na-Na, with the corresponding cross-correlations (Fig. 7C and Fig.7D), such as Na-Cl, O-Cl and O-Na. The self-correlations are to some extent included in the model, as they consist mainly of water-water and ion-ion correlations. However, the MD simulations capture the formation of small salt crystallites due to the interactions with the surrounding water, as shown in Fig.5. The O-O radial distribution function $g(r)$ resembles that of ice Ih, with the addition of disorder due to the water-brine interaction. Both the Cl-Cl and Na-Na correlations exhibit a peak at $r = 4\text{\AA}$ which is consistent with the atomic spacing at NaCl crystals where the FCC lattice spacing is $d = 5.64\text{\AA}$, and the shortest Cl-Cl and Na-Na distance is $d/\sqrt{2}$. The Na-Cl contains a dominating peak at $r = 2.8\text{\AA}$ and in addition two peaks at $r = 4.9\text{\AA}$ and 6.35\AA which correspond to the second and third Na-Cl in the salt crystal lattice.

The ion-water cross-correlations in the radial distribution function $g(r)$ contain information about the additional peaks not captured by the linear superposition model (Fig. 7D). Here, one can clearly distinguish the O-Cl and O-Na components, which is consistent with previous calculations in

NaCl aqueous solutions^{15,46}. One can understand these contributions as coming from an isolated ion (Na^+ or Cl^-) surrounded by water molecules. The first peak reveals the first neighboring water molecules around the ion, which in the case of Na-O corresponds to distances of $r = 2.45 \text{ \AA}$ and for Cl-O $r = 3.18 \text{ \AA}$. This difference is due to the influence of the positive charge of the Na^+ which attracts the oxygen, carrying a negative partial charge, and induces a major rearrangement of the hydration shells resulting to more packed local structure. In the case of Cl^- negative charge repels the surrounding oxygens and resulting in larger interatomic distances, which can also be affected by the larger ionic radius of Cl^- (1.67 \AA) in comparison to Na^+ (1.16 \AA). It was previously found that upon freezing the Cl^- ions are most favorably incorporated in the ice lattice by replacing two water molecules³². Thereby the ions included in the ice lattice will occupy fixed positions upon growth, imposed by the lattice symmetry and therefore the ion-water cross-correlation signal will be amplified. This is consistent with the hypothesis that the ion-water cross-correlations in the radial distribution function are responsible for the additional peaks observed in the diffraction pattern, that are not captured by the simple linear superposition model. From the MD simulations we can separate the O-Cl and O-Na contributions, that give rise to distinct diffraction peaks in the XRD pattern due to the different characteristic lengthscales observed in the cross-correlation part of the radial distribution function $g(r)$.

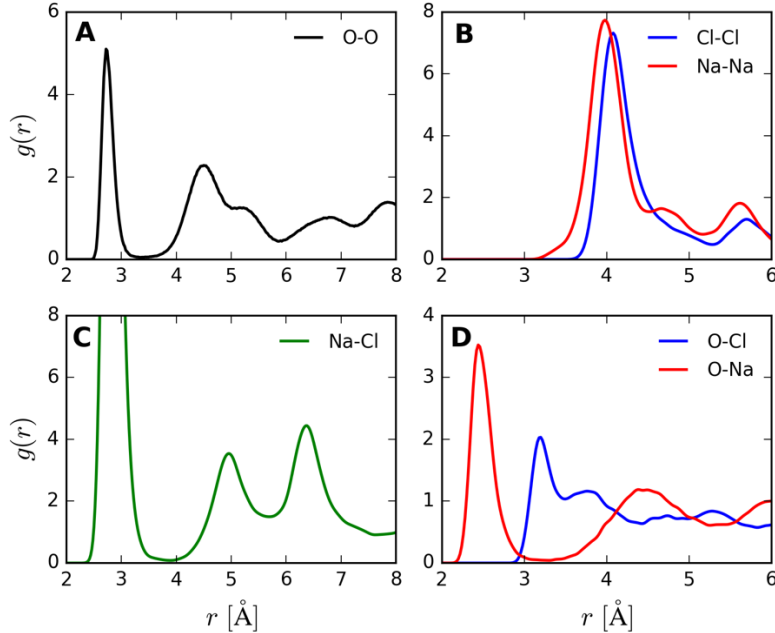


FIG. 7. The radial distribution function $g(r)$ obtained from the MD simulations. (A) The self-correlations between O-O and (B) Cl-Cl, Na-Na as well as the cross-correlations between (C) Na-Cl and (D) O-Cl, O-Na.

VI. CONCLUSIONS

In summary, we have investigated the crystallization of NaCl aqueous solutions using XRD for different temperatures (293 K to 230 K) and NaCl concentrations (0.86 M, 1.71 M, 2.57 M, 4.28 M). The brine rejection mechanism is discussed and we observe that a model consisting of a linear combination of the X-ray diffraction intensity of ice Ih crystals and NaCl aqueous solution reproduces well the experimental data and allows us to quantify the relative ratio between ice and brine at each condition. In addition, the regime where ice Ih coexist with NaCl crystals is analyzed. In this case a model consisting of two components, ice Ih and NaCl crystals, does not reproduce the observed diffraction pattern, which features additional peak contributions. In order to identify the origin of those additional components, we performed MD simulations of the NaCl aqueous solution crystallization process. The simulation results were analyzed in terms of radial distribution functions disclosing for both water-water, water-ion and ion-ion correlations. The analysis indicates that the additional peaks in the XRD pattern arise from the ion-water cross-correlation during the formation of salt crystallites and from ions

enclosed in the ice lattice. Furthermore, from the simulations we can estimate the concentration of ions trapped inside the ice, which is approximately 0.5% m/m. This value is reduced significantly from the initial NaCl concentration 2.3% m/m and is on the fresh water salinity limit, which is typically in the order of 0.1% m/m for drinking water and 0.5% m/m for agriculture.

The present investigation can give a valuable insight into the limitations of desalination based on freezing of salt solutions^{23–25} by providing a sensitive detection method of the ions trapped inside ice in the form of crystal impurities. One of the future investigations would be to study the desalination efficiency dependence on the nucleation rate, which from the current simulations is estimated to be in the order of 20 nm/ μ sec at 220K. It will be also interesting to spatially resolve spatially these defects by utilizing a nano-focus x-ray beam and quantify the size of the formed salt crystallites. Furthermore, it would be fascinating to probe the freezing in-situ with XRD, following the water-salt separation. One can achieve this by utilizing the novel x-ray free-electron lasers with high repetition rate, and thereby follow this process in real time and probe the dynamics with femtosecond resolution⁴⁷.

ACKNOWLEDGEMENTS

We would like to thank T.J Lane and K. Amann-Winkel for useful comments on the manuscript. The experiments were supported by Stockholm University and I.T. was additionally supported by the Erasmus+ program of the European Union. The simulations were performed on resources provided by the Swedish National Infrastructure for Computing (SNIC) at the National Supercomputer Centre (NSC) and the High Performance Computing Centre North (HPC2N).

REFERENCES

- ¹ P.G. Debenedetti, *J. Phys. Condens. Matter* **15**, R1669 (2003).
- ² C A Angell, (2003).
- ³ P. Ball, *Nature* **452**, 291 (2008).
- ⁴ A. Nilsson and L.G.M. Pettersson, *Nat. Commun.* **6**, 8998 (2015).
- ⁵ M. Chaplin, *Nat. Rev. Mol. Cell Biol.* **7**, 861 (2006).
- ⁶ P. Ball, *Proc. Natl. Acad. Sci.* **114**, 13327 (2017).
- ⁷ USGS, *Earth's Water Distribution* (n.d.).
- ⁸ P.K. Grover and R.L. Ryall, *Chem. Rev.* **105**, 1 (2005).
- ⁹ N.F.A. van der Vegt, K. Haldrup, S. Roke, J. Zheng, M. Lund, and H.J. Bakker, *Chem. Rev.* **116**, 7626 (2016).
- ¹⁰ D. Laage, T. Elsaesser, and J.T. Hynes, *Chem. Rev.* **117**, 10694 (2017).
- ¹¹ H.C. Allen and D.J. Tobias, *J. Chem. Phys.* **148**, 222501 (2018).
- ¹² W. Weeks and A. Assur, *THE MECHANICAL PROPERTIES OF SEA ICE* (1967).
- ¹³ M.M. Conde, M. Rovere, and P. Gallo, *J. Mol. Liq.* **261**, 513 (2018).
- ¹⁴ K. Winkel, M. Seidl, T. Loerting, L.E. Bove, S. Imberti, V. Molinero, F. Bruni, R. Mancinelli, and M.A. Ricci, *J. Chem. Phys.* (2011).
- ¹⁵ D. Corradini, M. Rovere, and P. Gallo, *J. Phys. Chem. B* **115**, 1461 (2011).
- ¹⁶ G. Camisasca, M. De Marzio, M. Rovere, and P. Gallo, *J. Chem. Phys.* **148**, 222829 (2018).
- ¹⁷ J.R. Espinosa, G.D. Soria, J. Ramirez, C. Valeriani, C. Vega, and E. Sanz, *J. Phys. Chem. Lett.* **8**, 4486 (2017).
- ¹⁸ G.D. Soria, J.R. Espinosa, J. Ramirez, C. Valeriani, C. Vega, and E. Sanz, *J. Chem. Phys.* **148**, 222811 (2018).
- ¹⁹ S. Woutersen, B. Ensing, M. Hilbers, Z. Zhao, and C.A. Angell, *Science* **359**, 1127 (2018).
- ²⁰ P.K. Rohatgi and C.M. Adams, *J. Glaciol.* **6**, 663 (1967).
- ²¹ K. Aagaard and E.C. Carmack, *J. Geophys. Res. Oceans* **94**, 14485 (1989).
- ²² A. Silvano, S.R. Rintoul, B. Peña-Molino, W.R. Hobbs, E. van Wijk, S. Aoki, T. Tamura, and G.D. Williams, *Sci. Adv.* **4**, eaap9467 (2018).
- ²³ J. Fournier, J.L. Grange, and S. Vergara, *Desalination* **15**, 167 (1974).

- ²⁴ P.M. Williams, M. Ahmad, B.S. Connolly, and D.L. Oatley-Radcliffe, *Desalination* **356**, 314 (2015).
- ²⁵ C. Xie, L. Zhang, Y. Liu, Q. Lv, G. Ruan, and S.S. Hosseini, *Desalination* **435**, 293 (2018).
- ²⁶ A.J. Wells, J.S. Wettlaufer, and S.A. Orszag, *Geophys. Res. Lett.* **38**, (2011).
- ²⁷ J. Weissenberger, G. Dieckmann, R. Gradinger, and M. Spindler, *Limnol. Oceanogr.* **37**, 179 (1992).
- ²⁸ Thomas, D. N. and G. S. Dieckmann, *Sea Ice 2nd Edition* (Blackwell, Oxford U. K., 2010).
- ²⁹ A. Křepelová, T. Huthwelker, H. Bluhm, and M. Ammann, *ChemPhysChem* **11**, 3859 (2010).
- ³⁰ T. Bartels-Rausch, H.-W. Jacobi, T.F. Kahan, J.L. Thomas, E.S. Thomson, J.P.D. Abbatt, M. Ammann, J.R. Blackford, H. Bluhm, C. Boxe, F. Domine, M.M. Frey, I. Gladich, M.I. Guzmán, D. Heger, T. Huthwelker, P. Klán, W.F. Kuhs, M.H. Kuo, S. Maus, S.G. Moussa, V.F. McNeill, J.T. Newberg, J.B.C. Pettersson, M. Roeselová, and J.R. Sodeau, *Atmospheric Chem. Phys.* **14**, 1587 (2014).
- ³¹ L. Vrbka and P. Jungwirth, *Phys. Rev. Lett.* **95**, 148501 (2005).
- ³² M.M. Conde, M. Rovere, and P. Gallo, *Phys. Chem. Chem. Phys.* **19**, 9566 (2017).
- ³³ J.S. Kim and A. Yethiraj, *J. Chem. Phys.* **129**, 124504 (2008).
- ³⁴ R. E. Dickerson, *Molecular Thermodynamics* (W. A. Benjamin, Pasadena, 1969).
- ³⁵ M.J. Abraham, T. Murtola, R. Schulz, S. Páll, J.C. Smith, B. Hess, and E. Lindahl, *SoftwareX* **1–2**, 19 (2015).
- ³⁶ W.L. Jorgensen, D.S. Maxwell, and J. Tirado-Rives, *J. Am. Chem. Soc.* **118**, 11225 (1996).
- ³⁷ W.L. Jorgensen, J. Chandrasekhar, J.D. Madura, R.W. Impey, and M.L. Klein, *J. Chem. Phys.* **79**, 926 (1983).
- ³⁸ C. Vega, E. Sanz, and J.L.F. Abascal, *J. Chem. Phys.* **122**, 114507 (2005).
- ³⁹ G. Bussi, T. Zykova-Timan, and M. Parrinello, *J. Chem. Phys.* **130**, 074101 (2009).
- ⁴⁰ H.J.C. Berendsen, J.P.M. Postma, W.F. van Gunsteren, A. DiNola, and J.R. Haak, *J. Chem. Phys.* **81**, 3684 (1984).
- ⁴¹ S. Bouazizi, S. Nasr, N. Jaïdane, and M.-C. Bellissent-Funel, *J. Phys. Chem. B* **110**, 23515 (2006).
- ⁴² R. Mancinelli, A. Botti, F. Bruni, M. A. Ricci, and A. K. Soper, *Phys. Chem. Chem. Phys.* **9**, 2959 (2007).
- ⁴³ I. Waluyo, D. Nordlund, U. Bergmann, D. Schlesinger, L.G.M. Pettersson, and A. Nilsson, *J. Chem. Phys.* (2014).
- ⁴⁴ C. Chen, C. Huang, I. Waluyo, T. Weiss, L.G. M. Pettersson, and A. Nilsson, *Phys. Chem. Chem. Phys.* **17**, 8427 (2015).
- ⁴⁵ W. Humphrey, A. Dalke, and K. Schulten, *J. Mol. Graph.* **14**, 33 (1996).
- ⁴⁶ Y. Ding, A.A. Hassanali, and M. Parrinello, *Proc. Natl. Acad. Sci.* **111**, 3310 (2014).
- ⁴⁷ F. Perakis, G. Camisasca, T.J. Lane, A. Späh, K.T. Wikfeldt, J.A. Sellberg, F. Lehmkuhler, H. Pathak, K.H. Kim, K. Amann-Winkel, S. Schreck, S. Song, T. Sato, M. Sikorski, A. Eilert, T. McQueen, H. Ogasawara, D. Nordlund, W. Roseker, J. Koralek, S. Nelson, P. Hart, R. Alonso-Mori, Y. Feng, D. Zhu, A. Robert, G. Grübel, L.G.M. Pettersson, and A. Nilsson, *Nat. Commun.* **9**, 1917 (2018).